Available online at www.sciencedirect.com
SCIENCE DIRECT®
Journal of Crystal Growth ▮ (▮▮▮▮) ▮▮▮–▮▮▮
JOURNAL OF CRYSTAL GROWTH
www.elsevier.com/locate/jcrysgro

Growth mechanism of atmospheric pressure MOVPE of GaN and its alloys: gas phase chemistry and its impact on reactor design

Koh Matsumoto[a,*], Akitomo Tachibana[b]

[a]*Marketing Div. Electronics, TAIYO NIPPON SANSO Corporation, Toyo Bldg. 1-3-26 Koyama, Shinagawa-ku, Tokyo 142-8558 Japan*
[b]*Department of Engineering Physics and Mechanics, Kyoto University, Kyoto 606-8501, Japan*

Abstract

In this paper, we present a model of the vapor-phase reaction of trimethyl-gallium (TMG), trimethyl-aluminum (TMA) and NH_3 and show our attempt to control parasitic reactions. First, we present a quantum chemical study of the unimolecular and bimolecular reactions of adducts. The direct adduct reaction pathway between TMA:NH_3 adducts can explain the reactivity of TMA. The calculated energy of each transition state for oligomer formation can well explain the experimental observation that TMGa:NH_3 adduct formation and cracking are reversible, and that TMA:NH_3 adducts react irreversibly to form higher-order oligomers.

Growth results for a reactor with and without recirculation flow are compared to show the importance of flow dynamics on the interaction between nanoparticles and precursors in the gas phase. Using a laminar flow three-layer configuration to ensure stable adduct injection, AlGaN with more than 17% Al can be uniformly grown over a 6-in-diameter platen at atmospheric pressure.

Keywords: A1. Gas-phase chemistry; A3. Chemical vapor deposition; A3. Metalorganic vapor phase epitaxy; B1. AlGaN; B1. GaN

1. Introduction

Atmospheric pressure or higher growth pressure is important for obtaining high-quality GaN and related alloys. The advantages of higher growth pressure on GaN MOVPE are as follows: (1) a smaller threading dislocation density (TDD) on sapphire [1–3], (2) better InGaN QW with a more coherent interface [4], (3) fewer nonradiative defects in GaN and better optical property [5,6], and (4) higher degree of Mg activation [7]. Thus, high-performance lasers and LEDs are obtained at 400 nm range [5,8].

However, parasitic reactions between TMA and NH_3 impede uniform and high Al content AlGaN

*Corresponding author. Tel.: +81-3-5788-8499; fax: +81-3-5788-8712.
E-mail address: kou.matsumoto@tn-sanso.co.jp (K. Matsumoto).

0022-0248/$ - see front matter © 2004 Elsevier B.V. All rights reserved.
doi:10.1016/j.jcrysgro.2004.08.115

growth at higher growth pressures [9]. It has been reported that the formation of adducts (Lewis acid–base complexes) between organometallics and NH_3, and the subsequent elimination of methane from such adducts, are the most probable reactions for oligomer formation [10,11]. By the gas-phase decomposition of $TMG/H_2/ND_3$, Mazzarese et al. have shown that the reaction by-product of TMG is solely CH_3D [11,12]. This demonstrates that the major pathway for methane elimination from TMG involves an adduct process very similar to that of the $TMG:AsH_3$ system [13]. At room temperature, Almond et al. [14] reported that the solid compound $(CH_3)_3Ga:NH_3$ eliminates methane to yield $(CH_3)_2Ga:NH_2$, which was found to exist in the trimer form $[(CH_3)_2Ga:NH_2]_3$. However, since TMG shows no appreciable evidence of parasitic reactions under normal growth conditions, it rarely forms higher-order oligomers in the vapor phase. Thon and Kuech [11] have also shown that $(CH_3)_2Ga:NH_2$ or $[(CH_3)_2Ga:NH_2]_x$ is thermally stable up to 500 °C and starts to decompose at higher temperatures. However, there has been no clear explanation for the very critical characteristics of the reaction of Al containing adducts until recently. Nakamura et al. [15] have studied the unimolecular and bimolecular adduct reaction pathways of organometallics and NH_3 by quantum chemical study. They calculated the transition state (TS) energy of the bimolecular reaction between adducts for oligomer formation. The TS energies for the TMA-related complexes are negative, while the TS energies for TMG is positive when we set the energy of individual molecules of organometallics and NH_3 to zero. From this result, $(CH_3)_3Ga:NH_3$ adducts will rather decompose again into individual molecules than go beyond TS when they are thermally excited. If two $(CH_3)_3Al:NH_3$ adducts are excited, they will easily go beyond TS rather than decompose into individual molecules. Makino et al. [16] also showed that $(CH_3)_3Al:NH_3$ adducts can be attached to this oligomer successively in the same manner.

Recently, Creighton et al. [17] have reported nanoparticle generation in MOVPE growth ambient. They have visualized by laser scattering that nanoparticles condense on the top of the thermal boundary layer. They have studied the appearance of the nanoparticle band as a function of temperature. The $(CH_3)_3Al:NH_3$ system showed nanoparticle generation at a relatively low temperature of ~200 °C. They also reported that $(CH_3)_3Ga:NH_3$ adducts form and decompose reversibly in a hot cell of FTIR, while $(CH_3)_3Al:NH_3$ irreversibly forms a higher-order oligomer, which was confirmed by observing the N–Al bond vibration mode. They proposed that nanoparticles are responsible for gettering precursors from growth ambient.

In the following section, we will describe the experimental features of the parasitic reaction of the TMG, TMA and NH_3 system, and the quantum chemical study of adduct reaction among them. Then, we will show growth experiments conducted using the reactor with and without recirculation flow to demonstrate the importance of flow dynamics on the parasitic reaction. Finally, we will show our attempt to control the parasitic reaction using a three-layer laminar flow gas injector with sheet separators.

2. Study of reaction of TMG–TMA–TMI–NH_3 system

2.1. Experimental characteristics of parasitic reaction

Fig. 1 shows AlN growth rate at atmospheric pressure as a function of growth temperature (T_g). AlN growth rate sharply dropped at a T_g higher than 500 °C. This shows that the parasitic reaction involving TMA requires some excitation energy to initiate the process. Since the upstream gas-phase temperature is far below the susceptor temperature, the on-set temperature of the parasitic reaction of the TMA–NH_3 system would be less than 500 °C. Fig. 2 shows AlGaN growth rate as a function of TMA input flow rate at a constant TMG flow rate. AlGaN growth rate decreased as TMA input flow rate increased. This implies that intermolecular collision has an important role in the enhancement of the parasitic reaction. The above results can be well explained if we assume

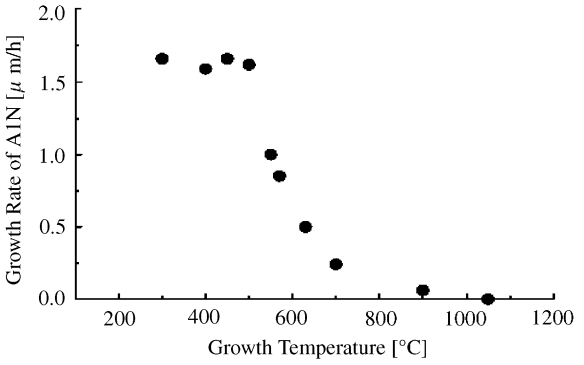

Fig. 1. AlN growth rate as a function of growth temperature (T_g). AlN growth rate sharply dropped at a $T_g > 500\,^{\circ}C$.

that nanoparticles are generated in vapor phase, as is proposed by Creighton et al. [17].

2.2. Quantum chemical study of organometals and NH_3

2.2.1. Bimolecular reaction pathway between adducts

Ab initio quantum chemical calculations were performed with the GAUSSIAN-94 program package [18]. The geometries of model reaction species and TSs for methane elimination were optimized by the analytical energy gradient method at the Lee–Yang–Parr gradient-corrected correlation functional [19] with the Becke's three hybrid parameters (B3LYP) [20], using double zeta basis set with the Hay–Wadt's effective core potential (ECP) [21,22] on metal atoms and Dunning–Huzinaga's full double-zeta Gaussian basis set [23] on the other atoms, called the LanL2DZ basis set. In this article, energy denotes enthalpy in kcal/mol.

First, the coordination interaction between organometallics and NH_3 is described. The $M(CH_3)_3$ molecule (**1**; each one, respectively, denotes **1a**, **1 g**, and **1i** for M = Al, Ga, and In, and so forth) forms a very stable complex with ammonia, $(CH_3)_3M{:}NH_3$ (**2**), due to the M–N coordinate bond through:

$$M(CH_3)_3\ (\mathbf{1}) + NH_3 \rightarrow (CH_3)_3M : NH_3\ (\mathbf{2}). \quad (1)$$

Fig. 3 shows a schematic drawing of reaction (1). As shown in the inset of Fig. 3, the stabilization energy of complex formation is the largest in the $TMA{:}NH_3$ system. Other details such as the charge transfer between the molecules and the treatment of TMA dimers are described in Ref. [15].

Because we mix organometallics and NH_3 in a relatively cool region before injecting them into the growth region in our reactor system (details are shown in a later section), it is possible to assume that all the organometallics are converted into adducts of the forms **2a**, **2 g** and **2i**. Therefore, we shall discuss here the intermolecular reaction between two complexes **2** and **2′** given as

$$(CH_3)_3M : NH_3(\mathbf{2}) + (CH_3)_3M' : (CH_3)_3\ (\mathbf{2'})$$

$$\rightarrow [\mathbf{TS1}] \rightarrow$$

$$(CH_3)_3MNH_2M'(CH_3)_2 \cdot NH_3\ (\mathbf{3}) + CH_4. \quad (2)$$

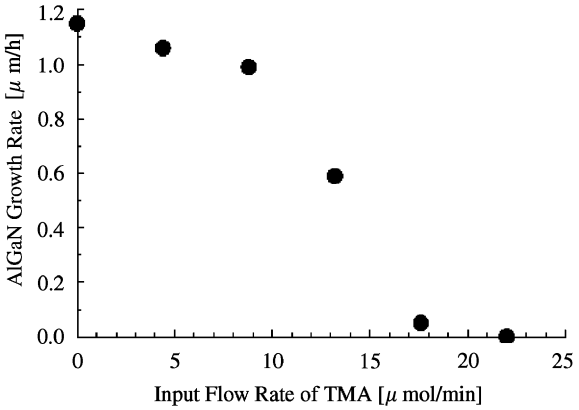

Fig. 2. AlGaN growth rate as a function of input TMA flow rate with a constant flow rate of TMG.

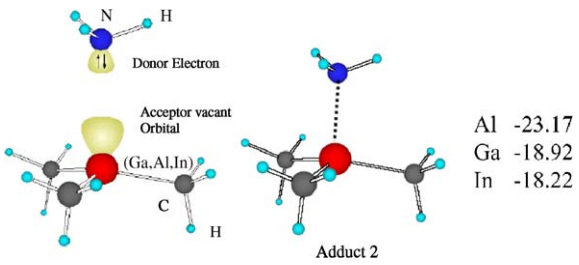

Fig. 3. $(CH_3)_3M$ and NH_3 forms a coordination bond without energy barrier. In the inset, the stabilization energy (kcal/mol) for the reaction $M(CH_3)_3 + NH_3 \rightarrow (CH_3)_3M \cdot NH_3$ is given.

The optimized geometry of TS1 as well as schematic reaction pathway is shown in Fig. 4. Table 1 summarizes the potential energy of the $M(CH_3)_3$:NH_3 system for the bimolecular mechanism, which is defined as a mechanism of methane elimination from two $M(CH_3)_3$-precursor-derived species, where the relative energies are standardized by setting the energy of the $M(CH_3)_3 + M'(CH_3)_3 + 2NH_3$ system to zero. When the combination of metals M and M′ are Al–Al, Ga–Al and Al–Ga, the TS1 values are −10.56, −5.51, and −2.90 kcal/mol, respectively. Since each potential energy is lower than zero, TS1 is favored more than the individual molecular state of TMG or TMA and NH_3. This means that the oligomer formation reaction would favorably proceed to **3**. The above results also suggest the formation of a type of oligomer similar to Al–N–Ga and Al–N–In in addition to that of Al–N–Al type. On the other hand, when the M–M′ combination is Ga–Ga, TS1 is 2.39 kcal/mol. This means that TMG:NH_3 adduct will more favorably decompose to individual molecules than be excited to TS1. For In–In combination, TS1 is −2.78 kcal/mol. Thus, it would be slightly more favorable for TMI to proceed to form oligomer **3**. Fig. 5 schematically illustrates this mechanism. In this adduct reaction process, please note that we require excitation energy from adduct state **2** to TS1. This explains that parasitic reactions to form nanoparticles require excitation energy. This also implies that it is advisable to mix organometallics and NH_3 in a cool region to reduce the energy of adducts to their ground states. When you mix organometallics and NH_3 in a hot region, adducts

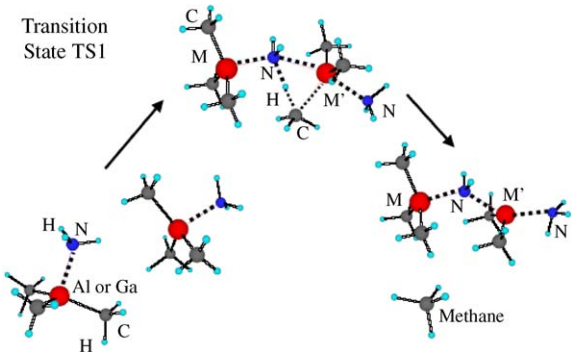

Fig. 4. Schematic of bimolecular reaction pathway between adducts.

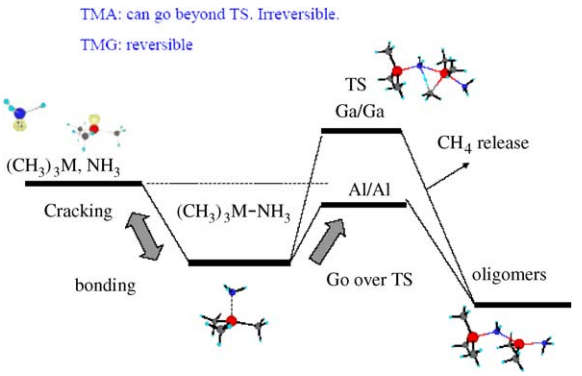

Fig. 5. If TS1 is larger than the starting molecular state, adduct **2** would be dissociated by thermal excitation. However, If TS1 is lower than the starting molecular state, they would go beyond TS1 to the oligomer state.

Table 1
Potential energy of $(CH_3)_3M$:NH_3 system for bimolecular reaction mechanism (kcal/mol)

$(CH_3)_3M:NH_3 + (CH_3)_3M':NH_3 \rightarrow (CH_3)_3M:NH_2M'(CH_3)_2:NH_3 + CH_4$

M/M′	Adduct	TS	Product
Al/Al	−46.34	−10.56	−68.82
Al/Ga	−42.09	−2.90	−61.63
Ga/Al	−42.09	−5.51	−63.80
Ga/Ga	−37.83	2.39	−56.74
Ga/In	−37.14	−3.19	−56.70
In/Ga	−37.14	2.93	−55.67
In/In	−36.45	−2.78	−56.15

The energy of the $(CH_3)_3M$ and NH_3 is set to zero.

remain excited and easily climb up the energy barrier to TS1, and generate oligomers. **2** can react with **3** and form higher-order oligomers in the same way as reaction (2) [16]. Following the above discussion, we can explain the experimental observations that TMGa:NH_3 adduct formation and cracking are reversible, and that TMA:NH_3 adducts react irreversibly to form higher-order oligomers. It is also noteworthy that we do not need to assume DMA–NH_2 monomer generation to initiate oligomer formation. TMA:NH_3 adducts readily climb up to TS1 through collisions in the vapor phase. This chain reaction easily occurs at upstream in a hot reactor.

2.2.2. *Uni-molecular reaction pathway for TMG decomposition*

Even though adduct **2g** for TMG easily decomposes at elevated temperatures, experimental results suggest that methane elimination from TMG is derived through adduct reactions [11,12]. Since the probability of collision between the two excited **2g** molecules is very rare, we will discuss the unimolecular elimination of methane from TMG under excess NH_3 condition. Under excess NH_3 condition, TMG forms a stable complex due to its coordination bond with two ammonia molecules, $H_3N{:}(CH_3)_3Ga{:}NH_3$ (**4**), without a potential energy barrier through:

$$\mathrm{Ga(CH_3)_3}\ (\mathbf{1}) + \mathrm{NH_3} \rightarrow \mathrm{(CH_3)_3M : NH_3}\ (\mathbf{2})$$

$$\mathrm{(CH_3)_3M : NH_3}\ (\mathbf{2}) + \mathrm{NH_3}$$

$$\rightarrow \mathrm{H_3N : M(CH_3)_3 : NH_3}\ (\mathbf{4}). \qquad (3)$$

The elimination of a methane molecule can occur in the presence of excess ammonia, by the intramolecular reaction of the complex **4** or the intermolecular collision between the complex **2** and an ammonia molecule.

$$\mathrm{H_3N : M(CH_3)_3 : NH_3}\ (\mathbf{4})$$

$$[\text{or } \mathrm{(CH_3)_3M : NH_3}\ (\mathbf{2}) + \mathrm{NH_3}] \rightarrow [\mathbf{TS2}]\ \ddagger$$

$$\rightarrow \mathrm{H_3N : M(CH_3)_2 : NH_2}\ (\mathbf{5}) + \mathrm{CH_4}. \qquad (4)$$

As shown in Fig. 6, the geometry of TS2 in the local part where the elimination of a methane molecule occurs is quite similar to that of TS1. Here, it is noteworthy that Bergmann et al. [24] observed a fragment of the molecule **4** by Q-MS spectroscopy. Fig. 7 shows the potential energy diagram of the $M(CH_3)_3{:}NH_3$ system for the unimolecular mechanism, which is defined as the mechanism of methane elimination from one $M(CH_3)_3$-precursor-derived species, where the relative energies are standardized by setting the energy of the $M(CH_3)_3 + 2NH_3$ system to zero. It is found that potential energy barrier is reduced through TS2 in the presence of excess ammonia for each $M(CH_3)_3 + 2NH_3$ system. In particular, the potential energy barrier for TMA is reduced to 4.67 kcal/mol (Table 2). Accordingly, it is considered that the gas-phase reaction of TMA proceeds rapidly in the presence of excess ammonia. Since the stabilization energy of the coordination by the second ammonia molecule (reaction

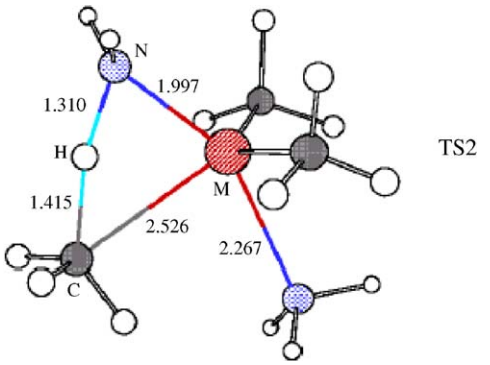

Fig. 6. Probable transition state of TMG decomposition pathway. Two NH_3 molecules are bonded under excess NH_3.

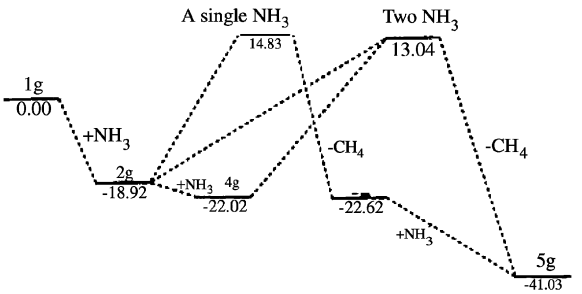

Fig. 7. Energy diagram for different NH_3 association numbers with TMG.

(3)) is relatively small, the mainstream of reaction (4) would be the intermolecular reaction between the complex **2** and an ammonia molecule together with the effective energy transfer due to the collision.

Recently, Hirako and Ohkawa have carried out a computer fluid dynamic simulation of the TMG–NH_3 system based on the quantum chemical calculation of each reaction step for a laminar flow horizontal reactor [25,26]. They have considered the detailed temperature distribution of the reactor wall and the wafer susceptor and incorporated the recent results of quantum chemical studies. They showed that the major reaction pathway for the first methane elimination occurs through a reaction path with both single NH_3 and two NH_3 associations. They also calculated reaction products and their special distribution as functions of growth pressure, and showed that the Ga–N molecule concentration near the substrate increases with growth pressure. In contrast to Ga–N, the DMGa–NH_2 monomer was another major by-product in the entire pressure range, and its concentration was almost constant regardless of growth pressure. The $(DMG{:}NH_2)_2$ concentration was very low and slowly increased with growth pressure. However, it did not show any abrupt jump as a function of growth pressure. The major conclusion regarding the species in the vapor phase seems to be coincident with what Mihopoulos and coworkers have reported previously in Ref. [10]. Sengupta showed that the $DMGa{:}NH_2$ concentration in the low-pressure MOVPE reactor was negligible and found only at the exhaust line, while most of the vapor-phase species were $TMG{:}NH_3$ adducts [27]. Both studies suggest that the parasitic reaction of TMG would not proceed very far by the unimolecular elimination of methane from **2g**. In the case that the parasitic reaction of TMG occurs, we will discuss it in the next section.

3. Design issue of MOVPE reactor

In the previous section, we described that TMA involving prereaction has very low activation energy in contrast to TMG. In this section, we will discuss the method of suppression of the upstream prereaction and the effects of flow dynamics on the growth of GaN and AlGaN. Fig. 8 shows a schematic drawing of the reactor used in this experiment. This reactor has a 180-mm-diameter platen which can handle $7 \times 2''$ wafers at a time (NIPPON SANSO SR-6000). The wafer susceptor is heated by a resistance heater and can be rotated on one axis. The TMG input flow rate was varied from 70 to 700 μmol/min. For GaN growth, the reactor pressure was set at 760 Torr. For AlGaN growth, the reactor

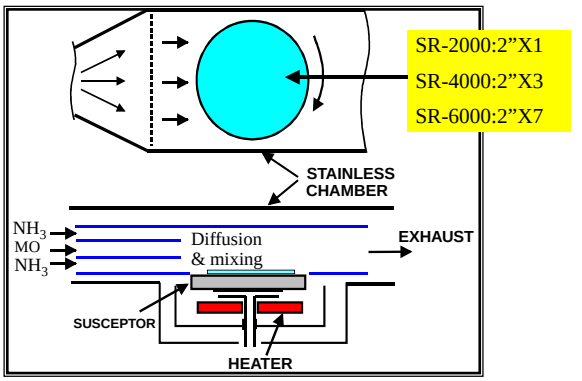

Fig. 8. Reactor #2 with a three-layer laminar flow gas injection system. (see text in detail).

Table 2
Potential energy for different NH_3 association number and excitation state for $M(CH_3)_3$ and NH_3

	Ground state (a) $(CH_3)_3M{:}NH_3$	Ground state (b) $H_3N{:}(CH_3)3M{:}NH_3$	TS of (a) with one NH_3 molecule	TS of (b) with two NH_3 molecules	Oligomer $H_3N{:}M(CH_3)_2$
$Al(CH_3)_3$	−23.17	−28.86	7.37	4.67	−49.86
$Ga(CH_3)_3$	−18.92	−22.02	14.83	13.04	−41.03
$In(CH_3)_3$	−18.22	−25.83	13.96	7.17	−35.26

TS energy decreases with an excess NH_3. All results are in kcal/mol.

pressure was varied from 300 Torr to 740 with a variable impedance control valve at the exhaust line of the reactor with a constant carrier gas flow rate. The typical carrier gas flow rates used were 70 l/min for GaN and 120 l/min for AlGaN. The NH_3 flow rate was kept constant with 15 l/min. A H_2/N_2 mixture of 50:50 was used as a carrier gas. The growth temperatures were 1150 °C for GaN and 1050 °C for AlGaN. Standard low-temperature GaN buffer technology was used to grow GaN. We compared two different reactors. In the first case, organometallics and NH_3 were mixed together at the inlet of the reactor. Judging from the wall deposit, there was unexpected recirculation in the reactor. By flow dynamic simulation, it was also confirmed that the reason for the recirculation was the improper design of the upstream flow channel in the part of flow expansion. We denote this reactor #1. Reactor #1 has no gas separators in the upstream flow channel. The other reactor is illustrated in Fig. 8 and denoted reactor #2. We have improved the reactor design to realize a laminar flow in reactor #2. In addition to this, we have employed a three-layer laminar flow gas injection system [28]. As shown in Fig. 8, organometallics and NH_3 are separately injected and mixed together by molecular diffusion. Under typical flow conditions, the spacing between the gas separators and their position are designed so that organometallics would diffuse laterally to the flow direction and reach the substrate surface just at the inlet of the growth region. Therefore, the mainstream of adduct $(CH_3)_3M{:}NH_3$ would be isolated by a sheath of gas stream from the heated reactor wall until it reaches the growth region.

Fig. 9 shows the growth rate variation of GaN in the flow direction for reactor #1. When the TMG input flow rate was below 400 μmol/min, the GaN growth rate variation along the flow direction was almost linear. The average growth rate with susceptor rotation was approximately 2 μm/h at this flow rate. Note that the growth rate variation of GaN with TMG supply rate of 700 μmol/min is a nonlinear function of wafer position. The GaN growth rate in downstream was almost zero for an input TMG of 700 μmol/min, which strongly suggests nanoparticle generation

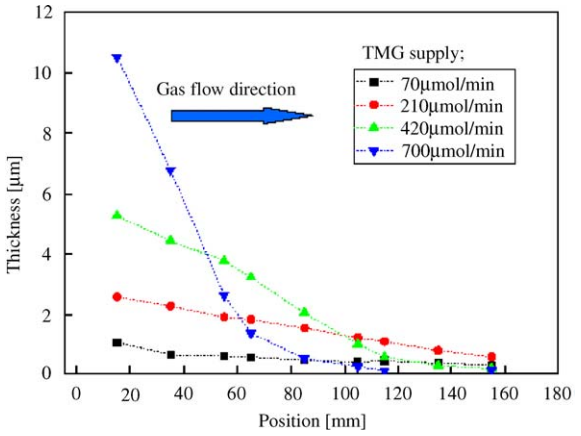

Fig. 9. Growth rate variation in flow direction for reactor #1 with recirculation.

by CVD mechanism [17]. Watwe et al. [29] have studied the gas-phase chemistry of TMG and NH_3 by quantum chemical calculation, and have shown that the $TMGa{:}(CH_3)_2GaNH_2{:}NH_3$ species has the lowest standard free energy activation barrier for methane elimination. If we assume that $(CH_3)_2GaNH_2$ is backdiffusing from downstream, this catalytic reaction will easily occur and proceed to oligomer formation. Once an oligomer starts to grow, nanoparticles would result by an iterative process. In the downstream region, most of the precursors would be consumed in the nanoparticle growth by CVD on the particle [17]. Although the decomposition velocity of $[(CH_3)_3Ga{:}NH_2]_x$ is determined by ambient gas-phase temperature, the growth rate of $[(CH_3)_3Ga{:}NH_2]_x$ is proportional to its collision frequency with TMG. Therefore, at some critical TMG input, $[(CH_3)_3Ga{:}NH_2]_x$ will start to grow. In this particular case, the growth rate of GaN showed saturation at approximately 2.5 μm/h. We must confine molecules such as $[(CH_3)_3Ga{:}NH_2]_x$ in the very vicinity of the crystal-growth surface to suppress nanoparticle generation. When we attempted to grow AlGaN with reactor #1 at atmospheric pressure, we failed because of a very strong parasitic reaction [30].

Fig. 10 shows the growth rate variation of GaN in the flow direction for reactor #2. A linearly decreasing growth rate along the flow direction was obtained for an input TMG flow rate as high

as 700 μmol/min. We have confirmed that GaN growth rate linearly increases with average growth rate up to 10 μm/h.

Fig. 11 shows the Al content in the solid phase as a function of input TMA/(TMA + TMG) for various growth pressures. AlGaN with an Al content of more than 20% has been grown at 740 Torr. The Al composition uniformity of $Al_{0.17}Ga_{0.83}N$ was ±3% over the 2-in-diameter wafer placed at one of 6 identical pockets on a 180-mm-diameter susceptor. Al incorporation efficiency has been more markedly improved than that in reactor #1, with which we could not grow

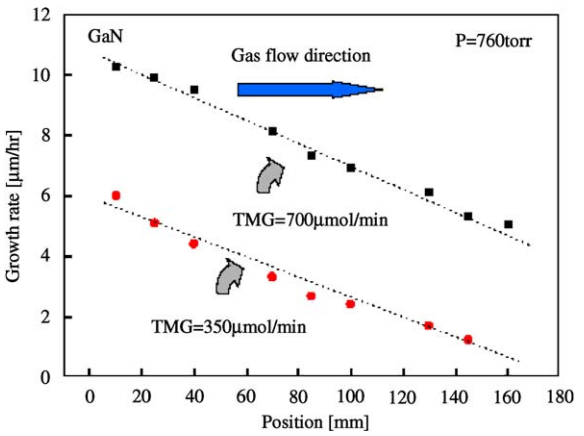

Fig. 10. Growth rate variation in flow direction for reactor #2 without recirculation.

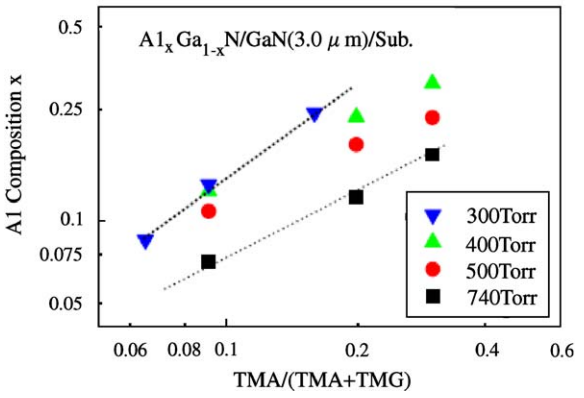

Fig. 11. Solid Al composition of AlGaN as a function of TMA/(TMA + TMG). Growth pressure was varied from 300 to 740 Torr. The line is a visual guide

any Al alloys at atmospheric pressure. In Fig. 11, note that Al incorporation efficiency increases as growth pressure decreases. At a growth pressure below 400 Torr, the Al content in the solid phase was larger than the input ratio of the vapor phase, while Al incorporation efficiency was less than one in the AlGaN films grown at 740 Torr. The result obtained at 740 Torr can be explained by the vapor-phase reaction of TMA and NH_3. However, the low-pressure result is not apparent from the viewpoint of the parasitic reaction. One possible reason for this would be the insufficient reaction time for TMG to decompose at low pressures. From the mechanism discussed in the previous section, the elimination of methane from TMA is much easier than that from TMG. Therefore, if the parasitic reaction is suppressed, Al is more easily incorporated than Ga at an extremely highspeed flow condition of more than 3 m/s. The selective desorption of Ga from the surface at high growth temperature is also a possible reason. Other details of AlGaN growth will be reported elsewhere [31]. By using a 120-mm-diameter susceptor reactor by the three-layer laminar flow gas injection system, a uniform AlGaN layer was also grown over 100-mm-diameter sapphire [32]. The degree of Al incorporation was constant as a function of growth pressure in this case. This discrepancy is supposed to arise from the fact that vapor-phase reactions involve complex interactions between adducts and their derivatives as well as higher-order oligomers. It is also important to consider the effects of thermophoretic force on reaction by-products and their special distribution. It will be particularly interesting to study the growth in the two-flow configuration invented by Nakamura in light of the findings presented here [33].

4. Summary

We have explained that the direct adduct reaction involving the TMA:NH_3 adduct is the most probable pathway for oligomer formation. The calculated energy of each transition state **TS1** to oligomer formation can well explain the experimental observation that TMGa:NH_3 adduct formation and cracking are reversible, and

$TMA:NH_3$ adducts react irreversibly to form higher-order oligomers.

A growth experiment using a reactor with recirculation flow showed a nonlinear GaN growth rate variation along the flow direction at a growth rate higher than 2 μm/h, while that using the laminar-flow three-layer gas injection reactor showed a linear growth rate variation even at a growth rate of 10 μm/h at atmospheric pressure. This demonstrated the importance of flow dynamics in the interaction between nanoparticles and precursors in the gas phase. By the three-layer injection configuration, AlGaN with an Al content of 17% with ±3% variation over a 2-in-diameter substrate placed in one of 6 identical pockets in a 6-in-diameter platen can be grown at 740 Torr. These results show the usefulness of quantum chemical analysis in improving reactor design for controlling parasitic reactions.

Acknowledgments

Quantum chemical calculation in this work was conducted as part of the graduate study of Drs. K. Nakamura and O. Makino of Kyoto University. The authors would like to thank the staff of NIPPON SANSO Corporation, H. Tokunaga, Y. Yano, and Dr. A. Ubukata and Dr. N. Akutsu for growth experiments and A. Yamaguchi, Dr. Y. Kitamura, T. Takahashi, K. Uematsu, and T. Yamazaki for the development of MOVPE equipment design. The authors would also like to thank Prof. K. Ohkawa of Tokyo University of Science for discussion about CFD and Prof. T. Egawa, Prof. M. Hao, Dr. H. Ishikawa, and M. Miyoshi (on leave from NGK INSULATORS Ltd.) of the Nagoya Institute of Technology for the development of the AlGaN growth process. This work is partially supported by a Special Coordination Fund for Promoting Science and Technology of the Japanese government.

References

[1] P. Finni, X. Wu, E.J. Tarsa, Y. Golan, V. Srikant, S. Keller, S.P. DenBaars, J.S. Speck, Jpn. J. Appl. Phys. 37 (Part 1, 8) (1998) 4460.
[2] A. Watanabe, H. Takahashi, T. Tanaka, H. Ota, K. Chikuma, H. Amano, T. Kashima, R. Nakamura, I. Akasaki, Jpn. J. Appl. Phys. 38 (Part 2 10B) (1999) 1159.
[3] K. Hiramatsu, K. Nishiyama, M. Onishi, H. Mizutani, M. Narukawa, A. Motogaito, H. Miyake, Y. Iyechika, T. Maeda, J. Crystal Growth 221 (2000) 316.
[4] K. Funato, S. Tomiya, S. Hashimoto, T. Miyajima, T. Kobayashi, Proceedings of the International Workshop on Nitride Semiconductors IPAP Conference Series, Vol. 1, p. 560.
[5] K. Yanashina, S. Hashimoto, T. Hino, K. Funato, T. Kobayashi, K. Naganuma, T. Tojyo, T. Asano, T. Asatsuma, T. Miyajima, M. Ikeda, J. Electronic Mater. 28 (3) (1999) 287.
[6] S. Shirakata, H. Miyake, K. Hiramatsu, Proceedings of the International Workshop on Nitride Semiconductors IPAP Conference Series, vol. 1, p. 109.
[7] P. Kozodoy, S. Keller, S.P. DenBaars, U.K. Mishra, J. Crystal Growth 195 (1998) 265.
[8] R.-C. Tu, C.-J. Tun, S.-M. Pan, H.-P. Liu, C.-E. Tsai, J.K. Sheu, C.-C. Chuo, T.-C. Wang, G.-C. Chi, I.-G. Chen, IEEE Photonic Tech. Lett. 15 (8) (2003) 1050.
[9] C.H. Chen, H. Liu, D. Steigerwald, W. Imler, C.P. Kuo, M.G. Craford, Mater. Res. Soc. Symp. Proc. 395 (1996) 103.
[10] T.G. Mihopoulos, Ph.D. Thesis, MIT, Cambridge, MA, 1999.
[11] A. Thon, T.F. Kuech, Appl. Phys. Lett. 69 (1) (1996) 55.
[12] D. Mazzaresse, A. Tripath, W.C. Conner, K.A. Jones, L. Calderon, D.W. Eckart, J. Electronic Mater. 18 (3) (1989) 369.
[13] G.B. Stringfellow, Organometallic Vapor-Phase Epitaxy: Theory and Practice, 2nd ed, Academic Press, New York, 1999.
[14] M.J. Almond, M.G.B. Drew, C.E. Jenkins, D.A. Rice, J. Chem. Soc. DALTON TRANS. (1992) 5.
[15] K. Nakamura, O. Makino, A. Tachibana, K. Matsumoto, J. Organometallic Chem. 611 (2000) 514.
[16] O. Makino, K. Nakamura, A. Tachibana, H. Tokunaga, N. Akutsu, K. Matsumoto, Appl. Surface Sci. 159–160 (2000) 374.
[17] J.R. Creighton, G.T. Wang, W.G. Breiland, M.E. Coltrin, J. Crystal Growth 261 (2004) 204.
[18] M.J. Frish, et al., GAUSSIAN-94, Gaussian Inc., Pittsburgh PA, 1995.
[19] C. Lee, W. Yang, R.G. Parr, Phys. Rev. Sect.B 37 (1988) 785.
[20] A.D. Becke, J. Chem. Phys. 98 (1993) 5648.
[21] P.J. Hay, W.R. Wadt, J. Chem. Phys. 82 (1985) 270.
[22] P.J. Hay, W.R. Wadt, J. Chem. Phys. 82 (1985) 299.
[23] T. H. Dunning Jr., P. J. Hay, in: H.F. Shaefer III (Ed.), Modern Theoretical Chemistry. Plenum, New York, 1976.
[24] U. Bergmann, V. Reimer, B. Atakan, Phys. Chem. Chem. Phys. 1 (1999) 5593.
[25] S. Tanaka, A. Hirako, K. Kusakabe, K. Ohkawa, ISBLLED-2004, Pb38, Korea, 2004.

[26] K. Kusakabe, A. Hirako, S. Tanaka, K. Ohkawa, Phys. Stat. Sol. (2004), Submitted for publication.
[27] D. Sengupta, J. Phys. Chem. B 107 (2003) 291.
[28] K. Uchida, H. Tokunaga, Y. Inaishi, N. Akutsu, K. Matsumoto, T. Itoh, T. Egawa, T. Jimbo, M. Umeno, Mater. Res. Soc. Symp. Proc. 449 (1997) 129.
[29] R.M. Watwe, J.A. Dumesic, T.F. Kuech, J. Crystal Growth 221 (2000) 751.
[30] H. Tokunaga, H. Tan, Y. Inaishi, T. Arai, A. Yamaguchi, J. Hidaka, J. Crystal Growth 221 (2000) 616.
[31] H. Tokunaga, A. Ubukata, Y. Yano, A. Yamaguchi, N. Akutsu, T. Yamasaki, K. Matsumoto, ICMOVPE-XII, Maui, J. Crystal Growth, (2004), Submitted for publication.
[32] M. Miyoshi, M. Sakai, S. Arulkumaran, H. Ishikawa, T. Egawa, T. Jimbo, M. Tanaka, H. Katsukawa, O. Oda, ICMOVPE-XII, Maui, J. Crystal Growth, (2004), Submitted for publication.
[33] S. Nakamura, Jpn. J. Appl. Phys. 30 (1991) 1620.